17. DEVELOPMENT OF ADVANCED NICKEL-TITANIUM-HAFNIUM ALLOYS FOR TRIBOLOGY APPLICATIONS

Sean Mills (CSM)
Faculty: Aaron Stebner and Mike Kaufman (CSM)
Industrial Mentors: Chris Dellacorte and Ron Noebe (NASA GRC)

17.1. Project Overview and Industrial Relevance

The high hardness, high compressive elastic strength and good corrosion resistance of ternary Ni-Ti-Hf alloys makes them optimum candidates for specialized bearing applications. In addition, aged NiTiHf alloys exhibit superelastic hysteresis curves under compressive loading and in torsion, as shown in **Fig. 17.1**. Conventional superelastic Ni-Ti alloys are known to experience high hardness and high residual stresses upon rapid quenching, resulting in cracking and machining distortion, whereas secondary precipitates can over-coarsen if cooled slowly, thereby reducing the material hardness. This project is designed to elucidate the effects of hafnium additions on the structure and properties of Ni-Ti-Hf alloys, with an emphasis on bearing element performance. It will be shown that hafnium additions have a significant impact on the transformation kinetics, which results in reduced residual stresses while retaining the high strengths and hardnesses that are desirable for bearing applications.

This multimodal study will include rolling contact fatigue characterization, residual stress and hardness measurement and time/temperature/transformation studies of selected NiTiHf alloys. Alloy optimization will be conducted by varying the nickel contents by 50.3 – 56 at. % and hafnium contents by 1 – 8 at. %. **Fig. 17.2** outlines the optimized alloy design space of the project that shows varied nickel and hafnium contents that will be investigated in the future. The sample compositions that have been tested in rolling contact fatigue are investigated via transmission electron microscopy (TEM) and are highlighted in previous work (**Fig. 17.2**), in addition to recent work (**Fig. 17.3**). Likely outcomes to the study include further understanding of rolling contact fatigue performance, failure mechanisms, performance (hardness, strength, lifetime predictions) versus residual stresses, and a map of alloy design space to allow for optimization of NiTiHf alloys for tribology applications.

17.2. Previous Work

17.2.1. Rolling Contact Fatigue

It is known that for nickel-rich compositions of NiTi, and also ternary NiTiHf compositions with low amounts of hafnium (~ 1 at. %), the Ni_4Ti_3 phase may be used for precipitation hardening without compromising the high hardness of the solid solution. In fact, the precipitates can also increase the hardness of the alloys. However, for NiTiHf with greater amounts of Hf (8 at. % or more), Hf and Ni rich "H-phase" precipitates form instead of Ni_4Ti_3 and provide even greater strengthening. ***Therefore, it is hypothesized that H-phase precipitation can also provide superior hardness, resulting in superior wear performance in alloys under rolling contact fatigue (RCF) conditions.*** Testing of NiTiHf samples using a three ball-on-rod set-up is imperative to ensuring this hardening behavior improves the component from an engineering standpoint.

A significant reduction in rolling contact fatigue performance has been observed in the $Ni_{54}Ti_{45}Hf_1$ alloy between 1.9 and 2.0 GPa. The brittle nature of spalling failures that are common in the specimens that failed at 2 GPa provide insight to the dominant failure mechanisms under Hertzian contact conditions [17.1]. ***Specifically, it was speculated that there must be a change in the uniaxial stress-strain behavior (for instance, the critical stress for martensite formation) in the range of 1.9-2.0 GPa that can be related to rolling contact fatigue performance.*** Thus, performing uniaxial compression testing on the same material as tested under RCF conditions was conducted to provide insight into the relationship between the critical contact stresses under fatigue conditions and the distinctive features on the stress-strain curves.

17.2.2. TEM Characterization

NiTiHf alloys with target compositions of $Ni_{56}Ti_{41}Hf_3$ and $Ni_{56}Ti_{36}Hf_8$ were made by induction-melting high-purity elemental constituents using a graphite crucible and casting into a copper mold. The ingots were homogenized in vacuum at 1050 ºC for 72 h and then extruded at 900 ºC at a 7:1 area reduction ratio. The extruded rods were sectioned into samples that were initially solution annealed at 1050 ºC for 30 minutes and water quenched. Samples of each composition were then pre-aged at 300 ºC for 12 h and air cooled, and finally aged a second time at 500 ºC for 4 h

and air-cooled. To isolate the effect of pre-aging on the functional properties of NiTiHf alloys, other test samples were directly aged at 550ºC for 4 h after the solution-anneal treatment (without pre-aging at 300ºC for 12 h). Conventional and high-resolution transmission electron microscopy (HRTEM), bright-field transmission electron microscopy and selected area electron diffraction microscopy of aged NiTiHf samples was carried out using an FEI Talos TEM (FEG, 200 kV). The TEM foils were prepared by electropolishing in an electrolyte of 30% HNO_3 in methanol (by volume) at around −35 ºC. To measure the average size and spacing of the H-phase and Ni_4Ti_3 precipitates in addition to observing precipitate morphology, several HRTEM taken from various regions were analyzed. A probe-corrected FEI Titan 1 was employed to take atomic resolution scanning transmission electron microscopy (HR-STEM) images of some of the microstructures. Digital Micrograph was utilized to extract diffraction information of the precipitates analyzed in the collected HRTEM and HR-STEM images.

Findings through these techniques indicate a significant change in microstructure and properties by adjustments in composition and secondary thermal processing. The effect of Hf shows a direct change in preference from one secondary precipitation type to another. **Fig. 17.3** clearly shows the change in morphology with respect to composition and aging conditions. At the 8 at. % Hf level, preference for fine H-phase precipitation provided means for higher toughness [17.2]. At the 3 at. % Hf level, preference for blocky Ni_4Ti_3 precipitation provided means for higher toughness in [17.3]. The effect of secondary processing via multi-step heat treatments show a change in the precipitates formed in a given sample. A two-step heat treatment of solution heat treatment and water quenching, and then a secondary aging step at 550 ºC before air-cooling reveals only one precipitate type.

17.3. Recent Progress

17.3.1. Rolling Contact Fatigue

Continued work on $Ni_{56}Ti_{41}Hf_3$ and $Ni_{56}Ti_{36}Hf_8$ alloys has been performed, which reveals consistent runout conditions (1.7E8 cycles) of the alloy at 2.0 GPa. At 2.1 GPa, the rods begin to spall and fail along the raceway. When compared with the binary $Ni_{55}Ti_{45}$ system under water quenching conditions, the air-cooled ternary alloy specimens are superior. However, when the higher Hf alloys are considered under water quenching conditions, the samples were successfully running to completion (1.7E8 cycles) at both the 1.9 and 2.0 GPa compressive stress levels. The improvement in fatigue performance is indicative that compositional adjustments (increasing hafnium levels slightly) and thermal processing via water quenching with additional higher temperature aging treatment play an important role in the longevity of the rolling contact fatigue specimens under compressive loads.

17.3.2. TEM Characterization of 56 at. % Nickel Alloys

More recent findings on $Ni_{56}Ti_{41}Hf_3$ and $Ni_{56}Ti_{36}Hf_8$ alloys indicate the origins of secondary precipitation and their effects on material hardness. **Table 17.1** includes the reported Ni_4Ti_3 and H-phase precipitate sizes, inter-particle distances in each specimen considered, and specimen hardness. To study the effect of pre-aging treatment, the microstructure of $Ni_{56}Ti_{36}Hf_8$ and $Ni_{56}Ti_{41}Hf_3$ alloys after being solution annealed and pre-aged at 300 ºC for 12 h was also investigated. **Fig. 17.4(a)** shows the BF-TEM micrograph and corresponding SAED pattern (inset) of $Ni_{56}Ti_{41}Hf_3$ alloy after pre-aging, confirming wide-spread blocky Ni_4Ti_3 precipitation. The size of the blocky Ni_4Ti_3 precipitates is approximately 65 ± 21 nm. Significant dark contrast surrounding the precipitates originate from the coherency strain fields around the precipitates.

Fig. 17.4(b) represents the BF-TEM micrograph of the pre-aged $Ni_{56}Ti_{36}Hf_8$ alloy, showing no clear precipitation within the grain. However, the corresponding SAED pattern (bottom left inset) shows faint spots corresponding to H-phase precipitates, similar to after the solution treatment condition. An additional SAED pattern provided in the upper right inset taken slightly off the [111] zone axis shows diffuse intensity patterns Moreover, the faint super reflections of H-phase precipitates are also included in the pattern containing diffuse intensities (top right inset). These diffuse intensities with periodical character in reciprocal space indicate the existence of short-range order in the real-space lattice. Such diffuse intensities have been reported in binary $Ni_{50.6}Ti_{49.4}$ after low-temperature aging, and are attributed to the existence of micro-domains in the form of clusters of Ni atoms as precursors to full formation of Ni_4Ti_3 nano-precipitates [17.4]. Analysis of diffuse intensities can help to determine the origin of the precipitate and its role in hardening. To obtain information before nucleation occurs, the selected area diffraction pattern in the upper right inset of **Figure 17.6(b)** was taken slightly off the $[111]_{B2}$ zone axis. The diffuse intensities appear more clearly in the higher index tilted zone in line shapes and show a periodic symmetry around the bright B2 reflections. This is indicative of

the existence of short-range ordering within the lattice as a precursor to widespread formation of H-phase. At the intersection of the lines and the Ewald sphere, spot-like intensities are more prominent [17.4], effectively producing the visible diffuse spots in the aligned $[111]_{B2}$ SAED pattern. Recently, Amin-Ahmadi et al. [17.5] reported the diffuse intensity after low temperature aging of $Ni_{50.3}Ti_{41.2}Hf_{8.5}$ (at. %) and related it to Hf and/or Ni atom clusters that form after low-temperature aging as a precursor to H-phase precipitation upon further aging at higher temperatures. Characteristic diffuse patterns taken in the $[122]_{B2}$ zone axis correspond to exclusive H-phase precipitation consist of a 60º / 120º angle relation branching periodically from the indexed <110> type spots [17.5]. In addition, bright triangular bright regions of intersection are visible in the H-phase diffraction pattern. The diffuse intensities observed in SAED pattern (top right inset of **Fig. 17.4(b)**) resemble the Ni or even Hf clustering for nucleation of both Ni_4Ti_3 and H-phase precipitates. **Fig. 17.4(c)** HR-TEM micrograph shows signs of changes in the B2 lattice, indicating short-range elemental segregation and micro-domain formation prior to any substantial precipitation event [17.4].

17.4 Plans for Next Reporting Period

- Continued work on rolling contact fatigue tests of optimized $Ni_{56}Ti_{36}Hf_8$ alloy.
- Continued microstructure characterization of 50-56 at. % Ni and 3-8 at. % Hf compositions for various heat treatments.
- TTT mapping through acquired TEM data and wide-angle x-ray scattering (WAXS) data to determine transformations in the NiTiHf system.
- Uniaxial compression testing of $Ni_{56}Ti_{41}Hf_3$ and $Ni_{56}Ti_{36}Hf_8$ alloys.

17.5. References

[17.1] C. Dellacorte , M.K. Stanford, T.R. Jett. Rolling Contact Fatigue of Superelastic Intermetallic Materials (SIM) for Use as Resilient Corrosion Resistant Bearings, Tribology Letters. 57.3 (2015) 1-10.

[17.2] B.C. Hornbuckle, R.D. Noebe, G.B. Thompson. Influence of Hf solute additions on the precipitation and hardenability in Ni-rich NiTi alloys, Journal of Alloys and Compounds. 640 (2015) 449-454.

[17.3] K. Otsuka, X. Ren. Physical metallurgy of Ti-Ni based shape memory alloys, Progress in Materials Science. 50.5 (2005) 511-678.

[17.4] S. Pourbabak, X. Wang, D. Van Dyck, B. Verlinden, D. Schryvers. Ni cluster formation in low temperature annealed Ni 50.6 Ti 49.4, Funct. Mater. Lett. 10 (2017) 1740005.

[17.5] B. Amin-Ahmadi, T. Gallmeyer, J.G. Pauza, T.W. Duerig, R.D. Noebe, A.P. Stebner. Effect of a pre-aging treatment on the mechanical behaviors of Ni 50.3 Ti 49.7-x Hf x (x 9at.%) Shape memory alloys, Scr. Mater. 147 (2018) 11-15.

17.6. Figures and Tables

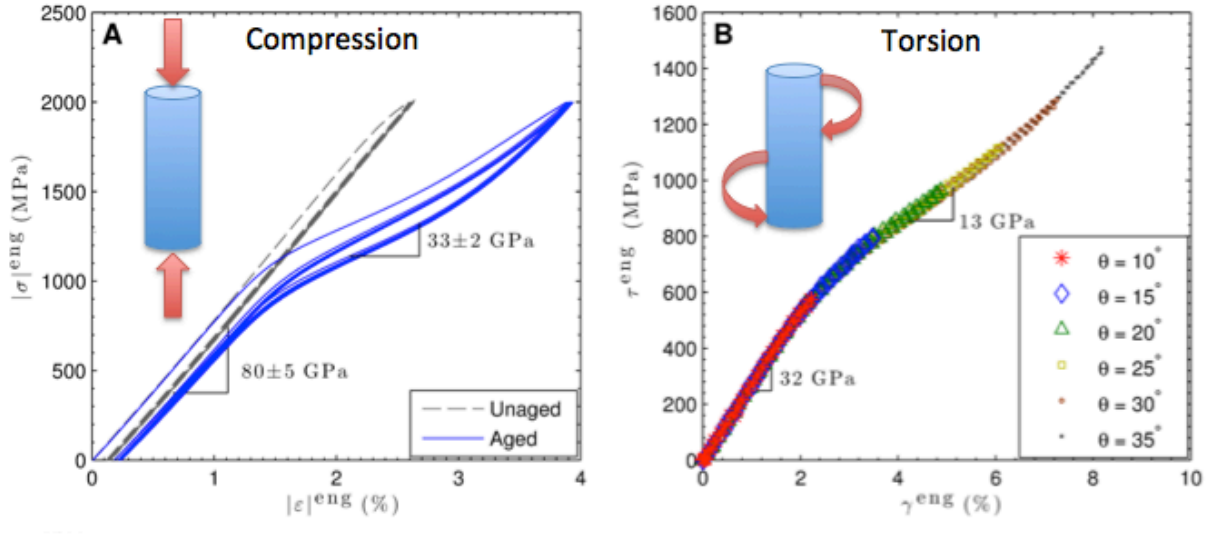

Figure 17.1: Superelastic hysteresis curves for aged NiTiHf under compressive loading and aged NiTiHf under torsional loading.

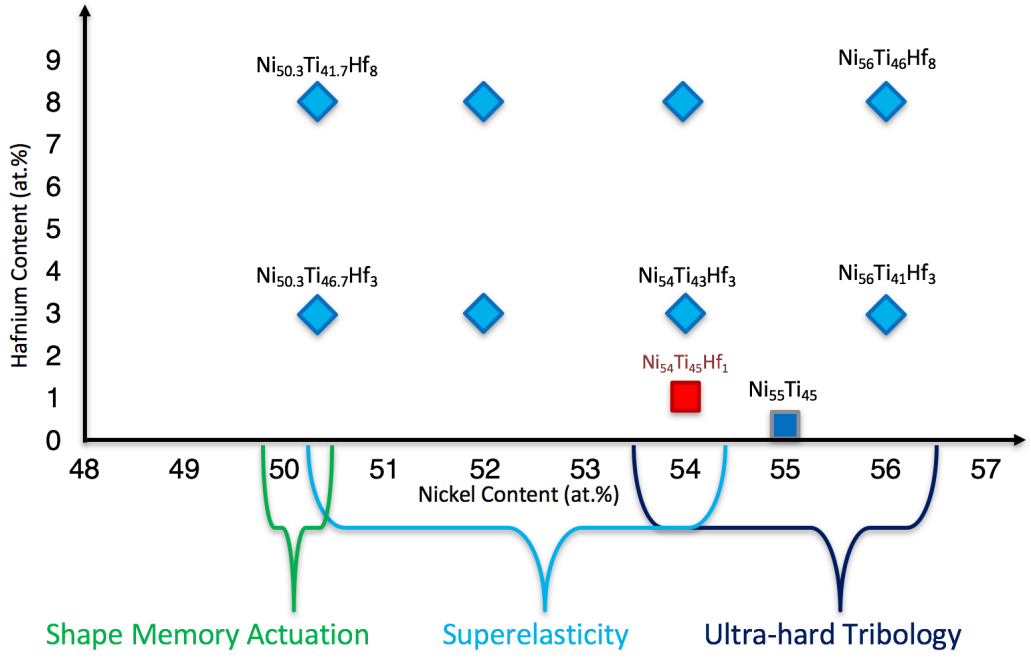

Figure 17.2: Target design space of NiTiHf alloys. CSM1–CSM8 samples vary in nickel and hafnium content. Their applicability as shape memory alloys (SMAs), superelastic alloys, and bearing alloys are listed.

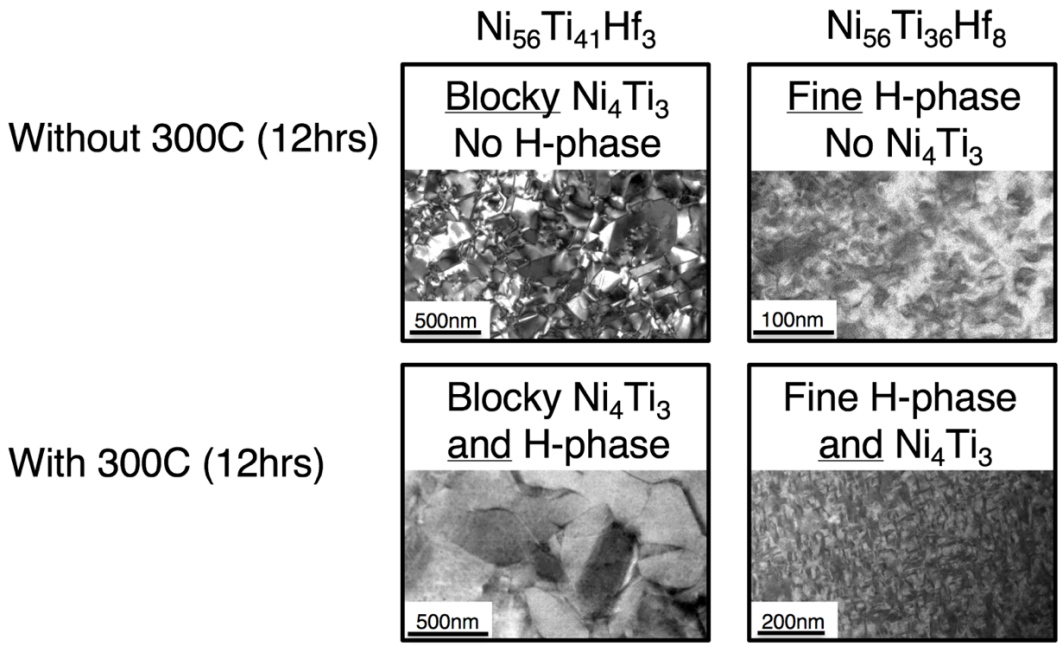

Figure 17.3: The preference for the type of secondary precipitation in Ni-rich NiTiHf alloys depends on changes in hafnium content and heat treatment. In order for both secondary precipitates to form within the microstructure, a 300ºC (12 h) pre-age is necessary.

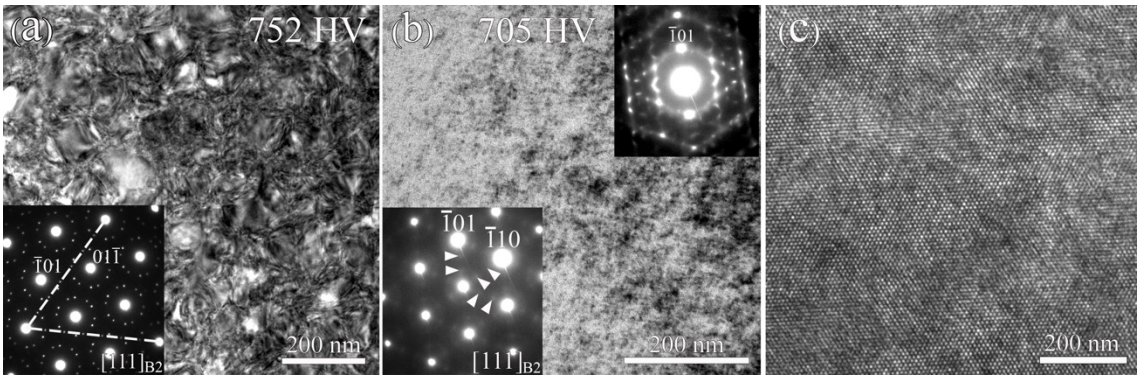

Figure 17.4 Conventional BF-TEM micrographs and corresponding SAED patterns after being solution annealed and pre-aged at 300 ºC for 12 h of (a) BF-TEM and SAED (inset) of $Ni_{56}Ti_{41}Hf_3$, clearly showing multi-variant blocky Ni_4Ti_3 precipitates and (b) BF-TEM and SAED (inset) of $Ni_{56}Ti_{36}Hf_8$ alloy, showing faint super reflection along 1/3<110> of H-phase precipitates. The top right inset shows an SAED pattern tilted off the [111] zone, revealing diffuse reflections corresponding to Hf and Ni clustering. (c) HR-TEM micrograph of the $Ni_{56}Ti_{36}Hf_8$ alloy, showing contrast changes that indicate micro-domains within B2 matrix.

Table 17.1 Ni_4Ti_3 and H-phase precipitate size / nearest neighbor distances with respect to hardness

Composition / HT	Ni_4Ti_3 Length (nm)	Ni_4Ti_3 Width (nm)	Ni_4Ti_3 distance (nm)	H-Phase Length (nm)	H-Phase Width (nm)	H-Phase distance (nm)	Hardness (HV)
$Ni_{56}Ti_{41}Hf_3$ / WQ	63 ± 16	63 ± 16	42 ± 13	**	**	**	707 ± 9
$Ni_{56}Ti_{41}Hf_3$ / WQ + 550(4 h)	113 ± 32	87 ± 19	92 ± 24	**	**	**	682 ± 10
$Ni_{56}Ti_{41}Hf_3$ / WQ + 300(12 h)	65 ± 21	65 ± 21	51 ± 19	**	**	**	752 ± 7
$Ni_{56}Ti_{41}Hf_3$ / WQ + 300(12 h) + 550(4 h)	138 ± 41	94 ± 23	105 ± 33	28 ± 4	13 ± 2	104 ± 13	710 ± 2
$Ni_{56}Ti_{36}Hf_8$ / WQ	**	**	**	2 - 5	2 - 5	N/A	716 ± 4
$Ni_{56}Ti_{36}Hf_8$ / WQ + 550(4 h)	**	**	**	21 ± 6	8 ± 2	17 ± 6	700 ± 7
$Ni_{56}Ti_{36}Hf_8$ / WQ + 300(12 h)	**	**	**	2 - 5	2 - 5	N/A	705 ± 8
$Ni_{56}Ti_{36}Hf_8$ / WQ + 300(12 h) + 550(4 h)	**	**	**	23 ± 5	12 ± 3	7 ± 2	769 ± 7

**Phase does not exist